Hindawi
Shock and Vibration
Volume 2022, Article ID 4999800, 16 pages
https://doi.org/10.1155/2022/4999800

Research Article

Study and Application of Rock Breaking Mechanism of Concentrated Water Hydraulic Smooth Blasting in Broken Sand-Stone Geological Conditions

Qingbiao Wang,[1,2,3,4] Xu Zhang,[2] Bin Gong,[5] Zhenyue Shi,[4] Yuanyuan Tian,[2] Dong Wang,[2] Zhongjing Hu,[4] Weiliang Sun,[6] Zhonghui Li,[6] and Wenxi Zhang[6]

[1]*College of Resources, Shandong University of Science and Technology, Tai'an 271019, China*
[2]*College of Civil Engineering and Architecture, Shandong University of Science and Technology, Qingdao 266590, China*
[3]*National Engineering Laboratory for Coalmine Backfilling Mining, Shandong University of Science and Technology, Tai'an 271019, China*
[4]*College of Safety and Environmental Engineering (College of Safety and Emergency Management), Shandong University of Science and Technology, Qingdao 266590, China*
[5]*College of Energy and Mining Engineering, Shandong University of Science and Technology, Qingdao 266590, China*
[6]*China Railway 14th Bureau Group 4th Engineering Co.Ltd, Jinan 250002, China*

Correspondence should be addressed to Zhongjing Hu; huyang@sdust.edu.cn

Received 21 February 2022; Accepted 16 March 2022; Published 1 April 2022

Academic Editor: Tao Meng

The use of polyenergy water pressure controlled blasting technology in tunnel construction is gradually being promoted, and the technology is often used in hard rock, and the mechanism of rock breaking in fractured sandstone strata is still lacking systematic research. The above mechanism was investigated using a combination of field experiments and ANSYS/LS-DYNA numerical simulation, and the results showed the following: (1) In the case of joint-hole blasting, the concentrating jet formed by the concentrating tube can effectively achieve controlled directional blasting of fractured sandstone. (2) The use of gun clay to seal the hole can effectively improve the stability of the blasting effect, reduce the waste of explosive gas, and effectively extend the duration of action. (3) The water bag enhances the blasting effect through the water wedge effect in the broken surrounding rock and also has the function of energy storage, which can effectively improve the blasting effect when combined with the gun clay. (4) The rock-breaking mechanism of polyenergy hydropressure smooth blasting in fractured sandstone geological conditions is the dual rock-breaking action of "polyenergy jet + water wedge action." (5) In this article, based on the analysis of blasting mechanism, the deployment method of polyenergy hydropressure smooth blasting is designed and has been well applied in engineering practice.

1. Introduction

In order to better enhance regional cooperation, the process of China's transportation construction has been accelerated, among which the construction of road and railroad tunnels under special geology is indispensable. The drill and blast method is the world's preferred method of excavation in rock tunneling. Based on the drill and blast method, the traditional smooth blasting technology was obtained. At this stage, the polyhydraulic blasting technology has evolved from the traditional smooth blasting technology. It has the advantages of convenience, high economic efficiency, and friendly to the surrounding environment.

Research on the drill-and-blast method has a wealth of research results. Verma et al. [1] obtained a large experimental data set of field parameters for the drill-and-blast method through field investigations and developed an empirical formula taken into account to assess rock damage around tunnels. Hamdi et al. [2] performed a numerical analysis of the damage evolution pattern caused by the

tensile blast of rocks and derived a dynamic tensile damage model for rocks. Monjezi et al. [3] used an artificial neural network (ANN) technique to construct a model for predicting blast vibration velocity and verified the feasibility of the model. Xie et al. [4] developed a rock tensile and compression-shear damage model that considered the effects of boundary conditions, in-situ stresses, and lateral pressure on directional cut blasting. Fan et al. [5] used the numerical manifold method (NMM) to simulate the velocity and attenuation law of stress waves propagating over tunnel cracks. Jiang et al. [6, 7] predicted the blasting damage characteristics of the surrounding rock by numerical simulation and ultrasonic testing methods and derived the damage zone and its calculation formula.

At this stage, domestic and foreign scholars for the tunnel smooth blasting technology have further in-depth research. Hu et al. [8] investigated the excavation process of smooth blasting and precracking blasting using dynamic cumulative blast damage numerical simulation technique. Feng et al. [9] used the finite element program ANSYS/LS-DYNA to simulate the blasting effect due to different spacing of tunnel blast holes. Zou et al. [10] analyzed the influencing factors of smooth blasting effect of rock tunnel using numerical simulation method from the perspective of weight. Zhou et al. [11] proved through experiments that the quality and flatness based on smooth blasting are better than presplitting blasting. Li et al. [12] innovatively and comparatively analyzed the formation of cracks between different delayed detonation light blast holes and different shaped detonation gun holes (PBH). Liu and Liu [13] proposed an improved optimization model for tunnel smooth blasting parameters built on the coupling of GA algorithm and ISVR algorithm. Li et al. [14] investigated the cracking process around adjacent gun holes using the time sequence control (TSC) method.

Polyenergy hydraulic smooth blasting technology is a further blasting technology derived from smooth blasting technology, which also has a large number of research results. Zhou et al. [15] verified that sandstone with higher water saturation possesses a lower fracture initiation point and damage rate during damage. Jiang et al. [16–18] studied the effect of water jets on rock fragmentation while concluding that the damage in the rock fragmentation zone is mainly due to plastic behavior. Huang et al. [19] demonstrated experimentally that controlled blasting of water pressure can effectively increase the water shock wave and bubble pulsation generated by blasting and improve the strain rate of the rock wall. Ye et al. [20] analyzed the mechanism of unloading pressure and increasing penetration in water pressure controlled blasting and concluded that the blasting effect is the product of the combined effect of blasting force and water pressure. Liu et al. [21] established an experimental rock fracturing system based on the foam flow continuity equation and the theory of high-pressure water jet impact pulling water wedge to break the rock. Wang et al. [22, 23] analyzed the dynamic properties of the media between 2 adjacent gun holes during directional controlled blasting. Wang et al. [24] proposed a continuous-interrupted hybrid method considering actual rock fragmentation and verified its ability to simulate blast fractures of indoor tests. Ding et al. [25] analyzed the energy release rate of blast-induced cracking and suggested that a reasonable decoupling factor could effectively improve the crushing effect. Lou et al. [26] introduced a star superposition model to derive the initial impact pressure on the well wall due to uncoupled charge blasting. Luo and Shen [27] conducted a preliminary study on the mechanism of cluster-controlled blast crack sprouting and extension in rocks, designed blast parameters, and performed field tests. Yin et al. [28] found that optimal blasting results could be obtained using decoupl bilateral slotted slot charge (BGSSC) blasting. Yan [29] further verified the rock-breaking mechanism of polyhydraulic blasting by experimental comparison. Liang et al. [30] found through their study that the blast fractures in both continuous and spaced polybursts were longer than in single-hole polybursts during polybursting. Li and Yang [31] applied the second generation of polyhydraulic smooth blasting technology in the Lower Gui Li Tunnel and obtained good blasting results. Song et al. [32] experimentally verified that multihole polyenergy blasting can effectively improve the degree of coal fracturing.

Numerous scholars have conducted a lot of research in the field of polyhydrodynamic smooth blasting, which has laid the theoretical foundation for subsequent research. However, the foremost engineering geological conditions studied are mostly hard or relatively hard rocks with good integrity. There continues to be a paucity of research on the mechanism and application of fractured sandstone geology to the breakage of fractured sandstone by concentrated hydrodynamic smooth blasting. To meet the requirements of tunnel blasting, this particular geological environment, research is necessary to fill the gaps in this research area.

Based on the Guantian Tunnel Project of Zhangjiajie-Jishou-Huaihua Railway, this article investigates the rock-breaking mechanism of concentrated hydropressure smooth blasting under fractured sandstone geological conditions using a combination of field experiments and numerical simulations with ANSYS/LS-DYNA software. The technology has been well applied in the Guantian tunnel project, providing a reference for similar projects and achieving good economic and social benefits.

2. Project Overview

In the new Zhangjiajie-Huaihua railroad tunnel project, the Guantian tunnel is located in the territory of Lancun Township, Mayang County, Hunan Province. The main line of the tunnel starts and ends at mileage DK211 + 349~DK215 + 126.27, with a design length of 3.7 km and a maximum burial depth of 167 m. There are many streams in the surface valleys of the tunnel site area, and the main water source has obvious seasonality. The tunnel is located in a weakly water-rich area, where the groundwater is mainly fractured water and nonerosive.

The distribution along this section is dominated by chalky soil, and the lithology is mainly muddy siltstone and powdery clay. Locally interspersed with maroon and yellowish brown gravel, some rocks contain ferromanganese

nodules. The project area is located in the tectonic uplift zone of the Huaxia system, with many large uplifts, depressions, and fractures and parallel to each other. As revealed by the tunnel's advanced geological forecast and geological exploration, the tunnel surrounding rocks are mainly mixed sandstone, weakly weathered, hard rock, fine grained, with more developed joints and partly filled with fissure calcareous. The surrounding rock around the tunnel is relatively broken as a whole, and the basic water content in the rock layer is low.

The tunnel is designed to be 1470-mm wide and 1238-mm high (Figure 1 for details). The energy-accumulating water pressure smooth blasting is used in tunnel excavation, and the blasting depth is strictly controlled. The step method cannot exceed the spacing of a steel arch per cycle footage. After the tunnel is excavated and formed, the initial support should be carried out in time and closed into a ring. The main support form of the initial lining section of the tunnel is the steel arch-anchor rod-anchor network support structure. The secondary lining is applied after the deformation of the tunnel surrounding rock and initial support is stabilized, and the formwork adopts an integral formwork cart and pumped concrete, which is formed in one time.

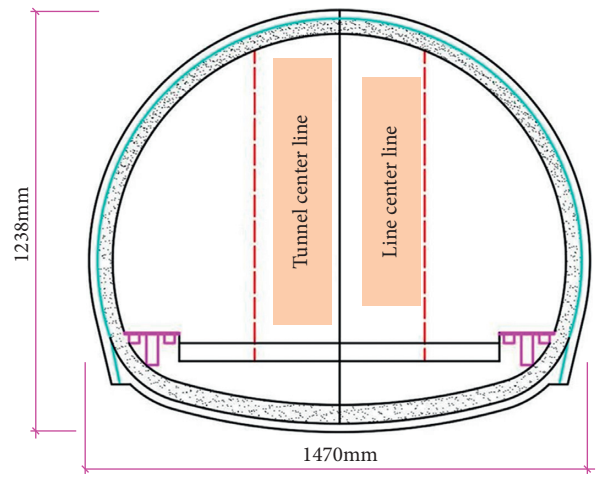

Figure 1: Tunnel section information.

3. Blasting Experiment

3.1. Experimental Scheme. The experiment was divided into two groups A and B for comparative blasting, where each group was set up with three gun holes for simultaneous detonation, and the designed experimental parameters are shown in Table 1 [16].

The experimental gun hole structure parameters are shown in Figure 2, and the specification type of each material used in the experiment (Table 2).

The physical experimental apparatus and materials are shown in Figure 3.

3.2. Hole Arrangement. As shown in Figure 4, the test gun hole was set with a diameter of 42 mm and a depth of 1.2 m. The gun hole points are laid on the same horizontal line on the palm face of the tunnel, and the direction of aggregation is horizontal for group A and vertical for group B.

3.3. Analysis of Experimental Results. As shown in Figure 5(a), the loading was completed in the laid out holes 1#, 2#, and 3# in accordance with the loading structure designed for group A experiments. The fissures in the surrounding rock at the palm face where this experiment is conducted are more developed, and a small amount of mud and sand is interspersed between the fissures.

As shown in Figure 5(b), the blasting surface of group A after blasting is flat, the blasting effect on the left side of hole 1# is not good, and the blasting depth is shallow compared with that of holes 2# and 3#. Holes 1#, 2#, and 3# produced more obvious through-length cracks in the polygraphic direction and smaller cracks in the nonpolygraphic direction.

As shown in Figure 5(c), the experiments borrowed the blasting effect of group B to form a comparison with group A and then analyzed the blasting effect of the process of polyhydraulic coupling holes blasting in depth.

As shown in Figure 5(d), the fissures in the surrounding rock at the blasting face of group B are more developed, and holes 4#, 5#, and 6# have produced more obvious fissures in the direction of vertical aggregation. The crack width is small compared with the effect of group A joint holes, and the crack length is also small, with a limited penetration effect on the surrounding rock. The cracks produced in the horizontal nonagglomerative direction are insignificant and far from penetrating.

As shown in Figure 6(a), the maximum cracks were produced near the gun holes in group A experiments, and the maximum crack widths were 4.03 mm, 4.05 mm, and 3.01 mm near gun holes 1#, 2#, and 3#, respectively. The length of the fracture at the edge of the 1# and 3# gun holes along the direction of aggregation is about 50 cm. The crack width in gun hole #2 is relatively large.

As shown in Figure 6(b), the maximum cracks were also produced near the gun holes in group B experiments, and the maximum crack widths were 3.01 mm, 2.30 mm, and 2.54 mm near gun holes 4#, 5#, and 6#, respectively. The fracture width of gun hole 4# is the largest, followed by gun hole 6#. The crack widths did not show obvious patterns in the spatial arrangement. The fracture extension length of the 5# gun hole along the direction of aggregation is the largest, about 38 cm.

The comparison between experimental data of group A and group B shows that the maximum crack width generated near the gun hole of group A is larger overall and the extension length of the crack is longer compared with group B. It shows that when the direction of energy concentration is the same as the direction of the gun hole arrangement (joint-hole concentration blasting), the energy concentration tube has better blasting effect.

In summary, the explosive detonation of non-concentration slot direction blasting produces a small

Table 1: Blasting test parameters.

Group	Charge structure	Hole number	Numbering	The direction of the condenser tube
A	Water bag + 60 cm tube + water bag + gun mud	3	1# 2# 3#	Level
B	Water bag + 60 cm tube + water bag + gun mud	3	4# 5# 6#	Erection

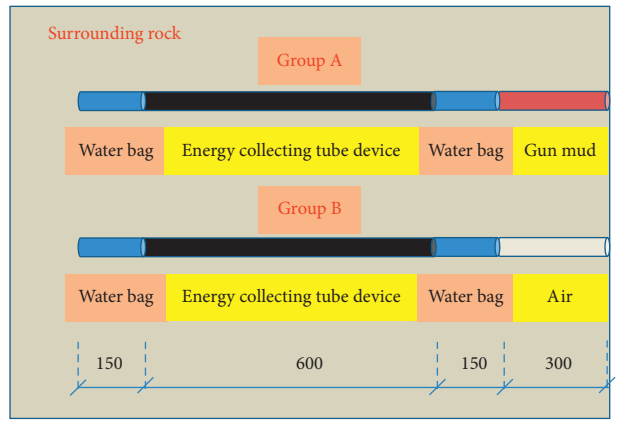

Figure 2: Dimensional parameters of gun hole charging structure (unit: mm).

Table 2: Estimating table of the material required for joint-hole plugging test.

Serial number	Name	Specification and type	Quantity	Remark
1	Nonelectric detonator	—	6	Ensure that all paragraphs are the same
2	Primacord	—	50	—
3	Blaster	—	1	—
4	V-shaped tube	φ 28.35, L 0.6 m	6	Filling 2 # rock emulsion explosive
5	Emulsified explosive	φ 32 mm-300 g	2	2 # rock emulsion explosive
6	Water bag	L 0.2 m	12	—
7	Stemming in drill hole	—	6	—

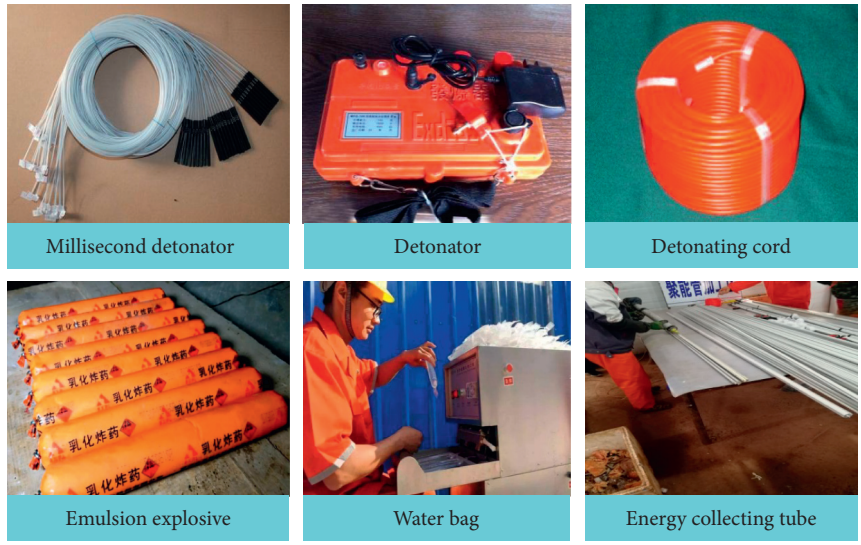

Figure 3: Instruments and materials for the experiment.

fissure. Due to the compression of the concentrator tube, a concentrator jet is formed in the direction of the concentrator tank. In the case of joint blasting, the concentrated jet can easily penetrate the rock to achieve the desired blasting effect, while less blast gas will propagate along with the existing fractures in the rock. This shows that controlled blasting of fractured sandstone can be achieved more effectively by joint-hole blasting with polytunneling.

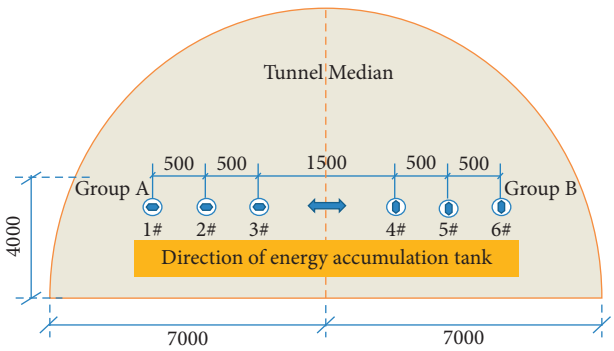

Figure 4: Arrangement of blasting hole in plugging blasting test.

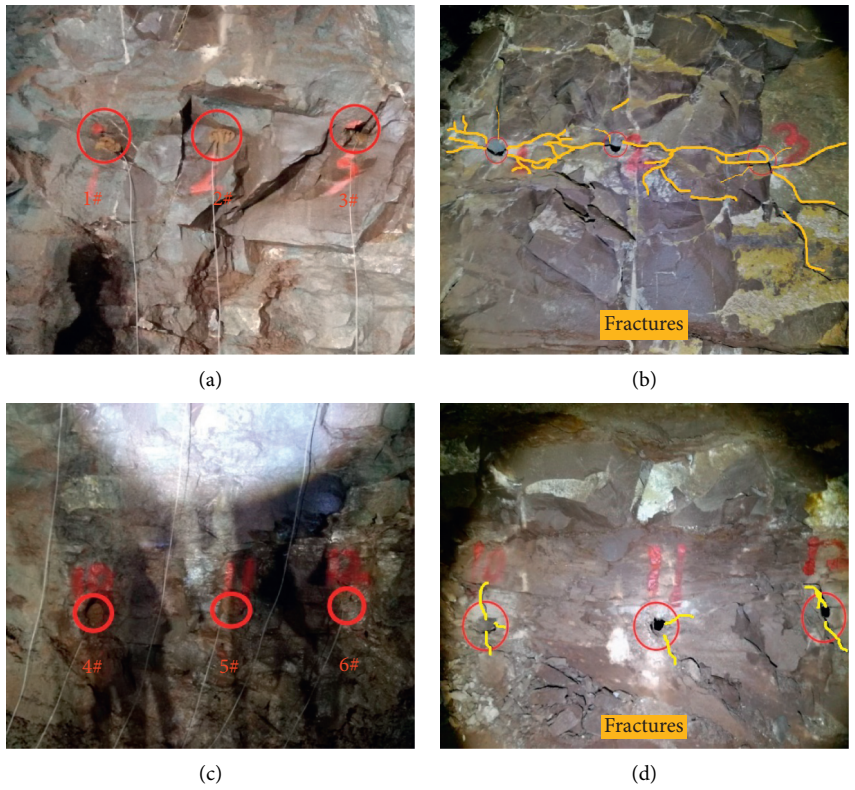

Figure 5: Effect before and after experimental blasting. (a) Effect of group A before blasting. (b) Effect of group A after blasting. (c) Effect of group B before blasting. (d) Effect of group B after blasting.

4. Numerical Simulation

The numerical simulation software ANSYS/LS-DYNA was used to establish a geometric model of a double-hole concentrated hydrodynamic smooth blast, modeled as a cylinder of radius $R = 200$ cm and height $H = 370$ cm. The model is laid out with 2 adjacent gun holes with a spacing of 50 cm, where the geometric model of the concentrator tube is shown in Figure 7.

In order to facilitate the visual quantification of the simulation results, two sets of monitoring points are fixed at equal distances in the finite element model for one side of the cannon hole in the direction of the concentrator slot and the direction of the noncollector slot. The number of monitoring points in each group is three, numbered as shown in Figure 8 above.

Due to the limited experimental conditions, the field experiments were conducted only for the analytical study of the aggregation effect of the aggregation tube. In order to verify the experimental results and to compensate for the experimental variables, the loading structures used in the numerical simulation are shown in Table 3.

4.1. Model Parameters. The LS-DYNA internal high-energy material intrinsic model HIGH_EXPLOSIVE_BURE material was chosen as the intrinsic model for the explosive simulation explosion process. Rock material parameters ∗MAT_Johnson_Holmguist_Concrete intrinsic material [33, 34]. The Gruneisen equation of state is used to describe the gas at high pressure. The detailed parameters of the air

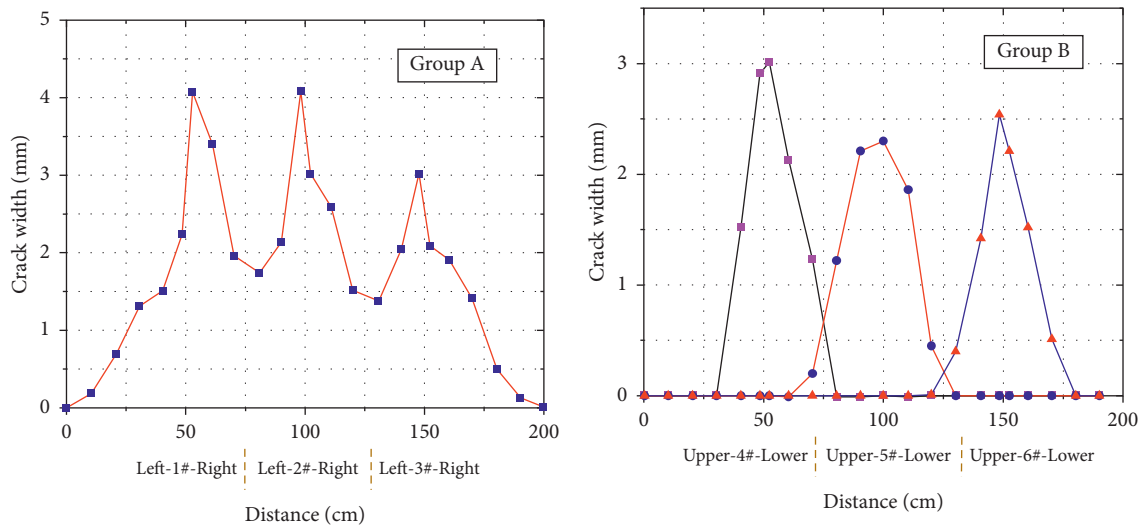

Figure 6: Crack width at different distances from the gun hole along the direction of energy concentration. (a) Group A. (b) Group B.

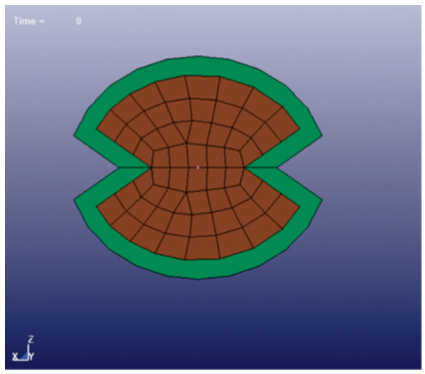

Figure 7: Geometric model of the condenser tube.

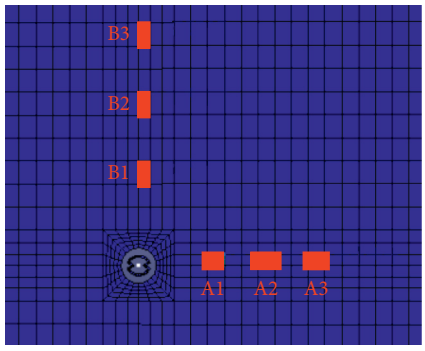

Figure 8: Selection locations of monitoring units and nodes.

material are shown in Table 4, and the air material parameter equation is gieven as

$$P = \frac{\mu C^2 \rho_0 \left[1 - \left((\gamma_0/2) - 1\right)\mu - (a/2)\mu^2\right]}{\left[1 - (S_1 - 1)\mu - S_2\left(\mu^2/\mu + 1\right) - S_3\left(\mu^3/(\mu+1)^2\right)\right]^2} + (a\mu + \gamma_0)E_0. \quad (1)$$

In the formula, ρ_0 is the material density, g/cm^3; γ_0 is the Gruneisen parameter; E_0 is the internal energy; C is the intercept of a curve; $S_1'S_2'S_3$ is the coefficient of curve slope; and a—γ_0, and μ first-order volume correction, $\mu = \rho/\rho_0^{-1}$

The intrinsic model of the water medium is chosen as the intrinsic model ∗MAT_NULL and the equation of state ∗EOS_GRUNEISEN is defined. The elastic-plastic material model defined as ∗MAT_PELASTIC was chosen for the polyenergy tube, and the detailed parameters are shown in Table 5.

4.2. Simulation Data Analysis. The stress clouds from this numerical model show that the stress waves simulated by blasting under all three charge configurations do not reach a peak at 6 ms. As the period continues to increase, the stress waves under the different charge structures begin to peak separately. Before 6 ms, the stresses under each charge structure in the same period are in the explosion development stage. To ensure that the selected different charge structures under the explosion stress in the same phase, so that the stress cloud has a better phase comparability. Therefore, the highest period for the stress cloud analysis is chosen as 6 ms in the following.

4.2.1. Simulation of Gun Mud-Shaped Charge. As shown in Figure 9, it is a schematic diagram of the structure of the polyhydraulic charge.

As shown in Figure 10, $T = 1.00$ ms, and the stress is a spherical wavefront, accompanied by the extended detonation of the explosive in the polygon tube from the bottom to the top; the stress propagates in a teardrop shape, and the surrounding rock is broken in a knife-edge shape. With T Ł 2.00 ms the double gun hole detonation at the stress wave overlap superposition, the bottom of the water bag at the formation of the spherical wavefront, the water-energy is stored rapidly, the pressure gradually increased. $T = 4.00$ ms

Table 3: Simulation charge scheme.

Group	Charge structure	Initiation site	The direction of energy sink
1	Water bag + tube + water bag + gun mud	Bottom hole	Identity
2	Water bag + tube + water bag + air	Bottom hole	Identity
3	Air + concentrator + air + gun mud	Bottom hole	Identity

Table 4: Air medium material parameters.

Parameter	R_0 (kg/m^3)	C_0	C_1	C_2	C_3	C_4	C_5	C_6	Eo (GPa)	V_0
Numerical value	1.30	0	0	0	0	0.41	0.41	0	2.49E5	1.1

Table 5: Polyenergy tube parameters.

Materials	Modulus of elasticity (GPa)	Density (g/cm^3)	Poisson's ratio	Shear modulus (GPa)	Yield stress (MPa)
PVC	3.2	1.45	0.37	1.2	2400

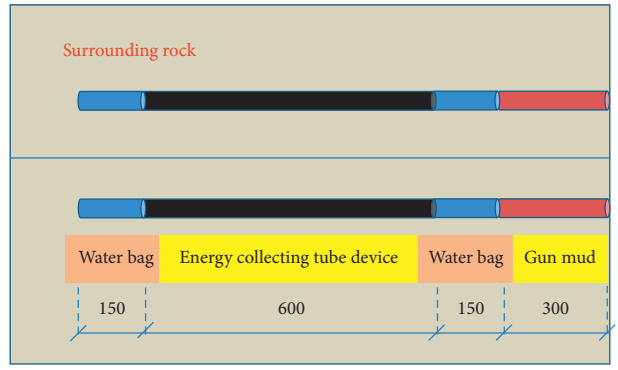

Figure 9: Schematic diagram of gun mud-accumulating charge structure.

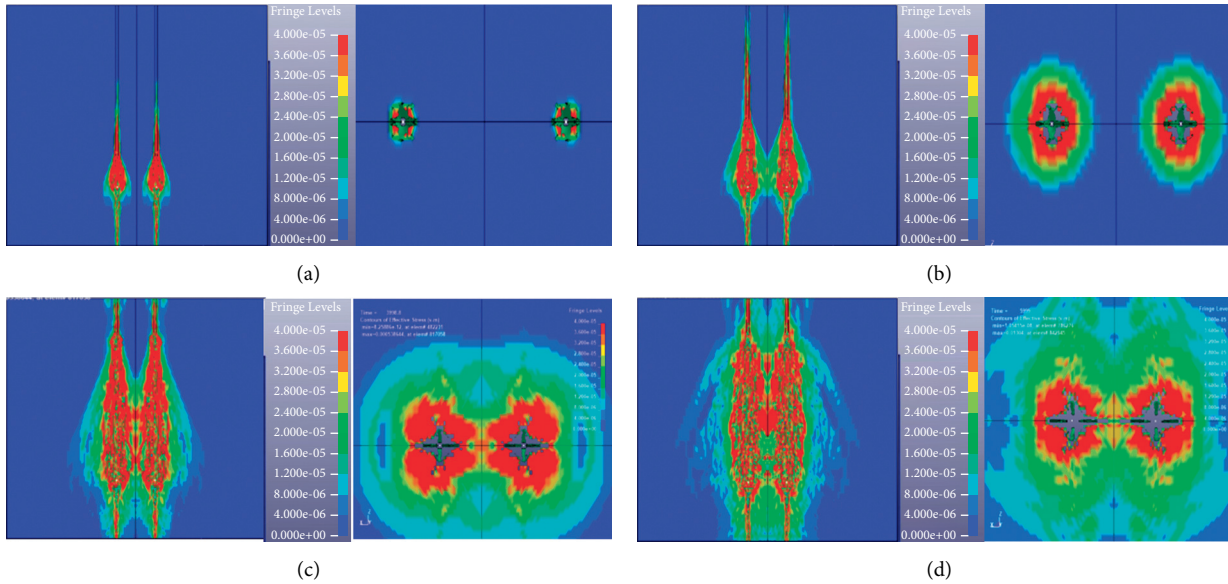

Figure 10: Stress nephograms of vertical section and lateral section of smooth blasting with mud-accumulated hydraulic pressure (unit: 10^5 MPa). (a) $T = 1.00$ ms. (b) $T = 2.00$ ms. (c) $T = 4.00$ ms. (d) $T = 6.00$ ms.

when the blast stress wave propagates to the topwater bag, which is obviously hindered by the polygon tube during the diffusion of the stress wave along the direction of the polygon, and the polygon tank begins to convert the kinetic energy generated by the blast into high-pressure, high-energy potential energy. When $T = 6.00$ ms, the blasting stress wave basically completes the diffusion, and the stress shows a stable ellipsoidal shape. With the passage of time, the stress

begins to spread continuously, and the rock cracks tend to stabilize after expanding to the maximum value, at which time the stress-strain generated by blasting approaches the end.

4.2.2. Mudless-Shaped Charge Structure Simulation. As shown in Figure 11, a schematic diagram of the gun clay-free-charge structure is shown.

As shown in Figure 12, when $T = 1.00$ ms, the detonation produces a spherical wavefront, the stress wave at the detonation location shows a teardrop shape, the stress is further generated and transmitted to the direction of the gun hole orifice, and the stress wave state is similar to the propagation range when gun clay is used to seal the hole. When $T = 2.00$ ms, the stress is propagated in the form of water droplets, and a spherical wavefront appears at the bottom water pocket, and the state of the stress wave is similar to that when the hole is sealed with gun clay, and the stress waves in the two shell holes overlap. When $T = 4.00$ ms, the stress wave began to propagate to the hole, and the state of the stress wave presented as a spindle shape; at this time, the concentration tube concentration slot location began to gather energy, but the energy gathered compared with the use of gun clay to seal the hole is slightly insufficient, and the blast wave continues to spread to the location of the hole. When $T = 6.00$ ms, the stress wave diffusion formed an ellipsoidal shape and began to stabilize, and the side profile stress cloud showed that the energy gathering process of the polygon tube was not obvious, and the blast fracture was small. Due to the reduced blasting compressive stress, the water wedge effect appears to be discounted and enters the weakening phase earlier compared with the case with gun clay sealing the shell hole. At the same time, the stress fracture formed in the direction of the gun hole aggregation is smaller compared with that with gun clay sealing, and the fracture cavity formed in the nonaggregation direction is larger.

4.2.3. Simulation of Anhydrous Bag-Accumulating Charge Structure. As shown in Figure 13, a schematic diagram of the anhydrous bag-poly charge structure is shown.

From Figure 14, it can be seen that at $T = 1.00$ ms, the detonation site is a spherical wavefront, and the stress propagates to the top of the gun hole in a teardrop shape, with a reduced force wave propagation range compared with hydrodynamic blasting. When $T = 2.00$ ms, the wavefront surface formed after the stress wave propagates to the bottom surface is smaller, indicating that the stress propagates more efficiently in the water than in the air. When $T = 4.00$ ms, the stress wave basically propagates to the top air section; at this time, the transverse width of the wavefront surface in the air section does not appear to increase but continues to propagate to the whole mouth gun clay in the form of water droplets. When $T = 6.00$ ms, the stress wave spread to form an elliptical shape and tends to stabilize, then, the explosion generated by the stress effect gradually weakened.

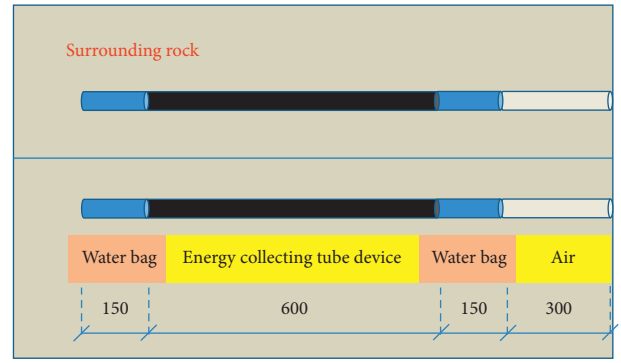

Figure 11: Schematic diagram of structure without gun clay-poly charge.

5. Analysis of Experimental Results

As shown in Figure 15, the maximum value of stress was measured to be about 10.8 MPa in the nonconcentration direction. In the concentration trough direction, the maximum value of stress was measured to be about 25.3 MPa.

As shown in Figure 16, the maximum value collected in the nonconcentration direction is about 15.9 MPa. The maximum value of stress measured in the concentration direction is 23.1 MPa. Compared with the hydraulic blasting case with gun clay blockage, the effective stress in the direction of energy concentration is reduced. The effect of polyenergy blasting is worse than the case with clay blockage. Description of blocking gun clay can effectively prevent the burst of raw gas released at will, to enhance the aggregation effect of the aggregation tube.

As shown in Figure 17, the maximum value of stress measured in the direction of the nonconcentration is about 10.4 MPa. In the direction of the concentration, the maximum stress measured in cell A1 is about 23.7 MPa.

The maximum value is reduced compared with the polyhydraulic blasting. This indicates that the presence of water bags can increase the stress generated by blasting on the peripheral holes within a certain range. The water bag has a significant effect of spreading stress compared with air.

The above threeThe above three . . . energy jet impact" for clarity. Please confirm that this is your intended meaning."? charge structures show that the location where the stress is generated maximum in the direction of concentrated energy is the A1 monitoring point (i.e., the maximum is generated near the gun hole), which is consistent with the principle of concentrated energy jet impact. Nongathering direction and no gun clay-charge structure stress maximum generation location for B1 monitoring point. The other two charge structure maxima are generating at monitoring point B2. It indicates that the penetration ability of blasting response in the nonagglomerative direction surrounding rock is reduced when no gun clay is used to seal the hole.

As shown in Figure 18, the blasting stress was monitored early in the surrounding rock during waterless bag blasting. It shows that water bag has certain energy storage function. In the process of blasting without mud, the maximum stress action time is greatly shortened. The maximum stress value is relatively small, and the energy is wasted. It shows that

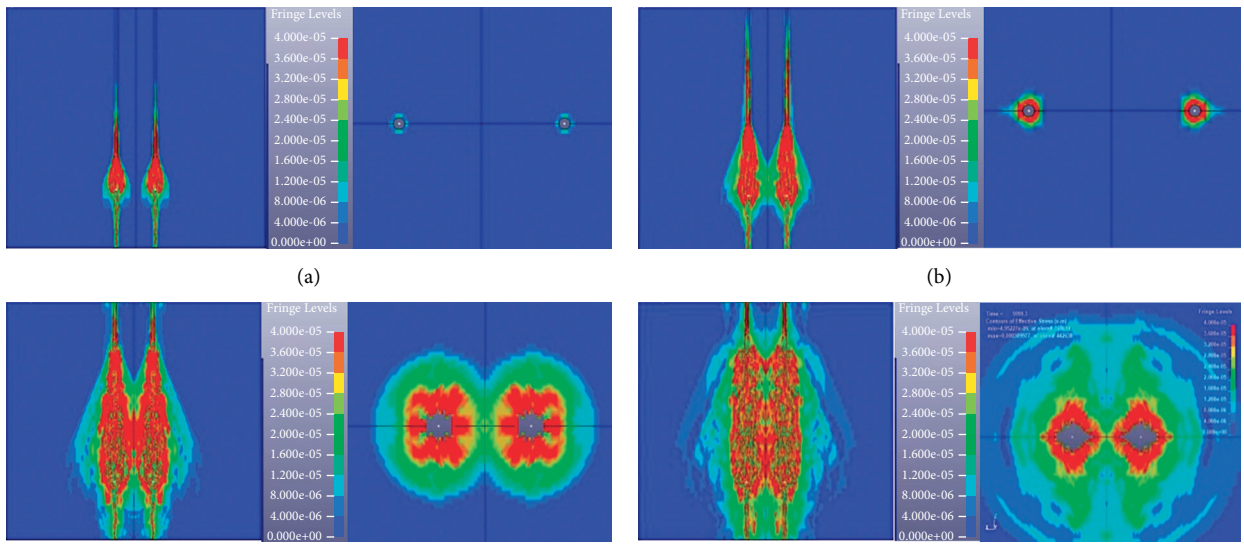

Figure 12: Stress nephograms of prone section and side section of concentrated hydraulic smooth blasting (unit: 10^5 MPa). (a) $T = 1.00$ ms. (b) $T = 2.00$ ms. (c) $T = 4.00$ ms. (d) $T = 6.00$ ms.

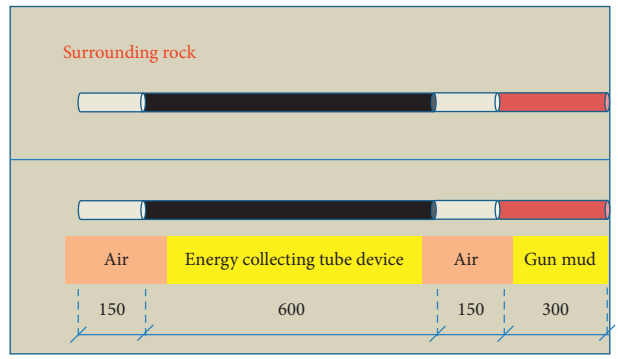

Figure 13: Schematic diagram of no gun mud-shaped charge structure.

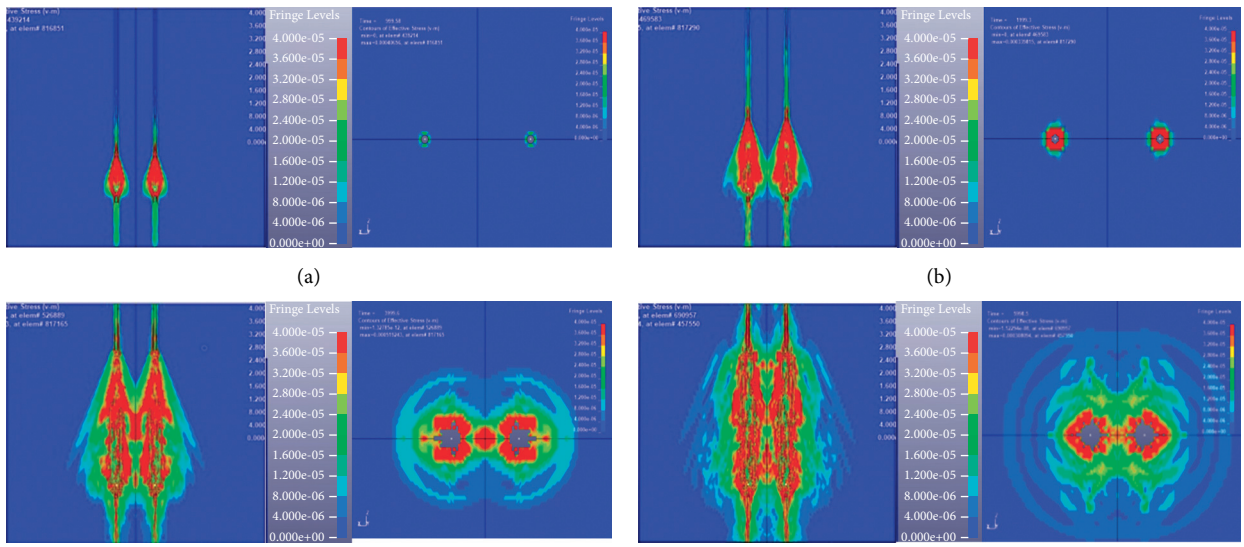

Figure 14: Stress nephograms of prone section and lateral section of anhydrous bag-accumulator smooth blasting (unit: 10^5 MPa). (a) $T = 1.00$ ms. (b) $T = 2.00$ ms. (c) $T = 4.00$ ms. (d) $T = 6.00$ ms.

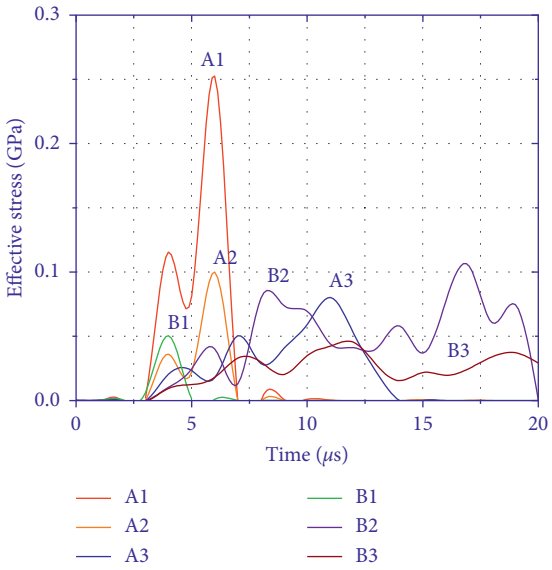

Figure 15: Stress curve of hydraulic charge blasting unit.

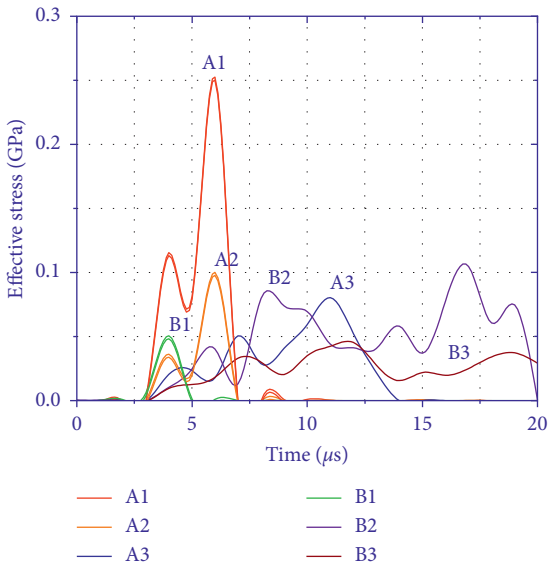

Figure 16: Stress curves of nonshot mud-charge blasting unit.

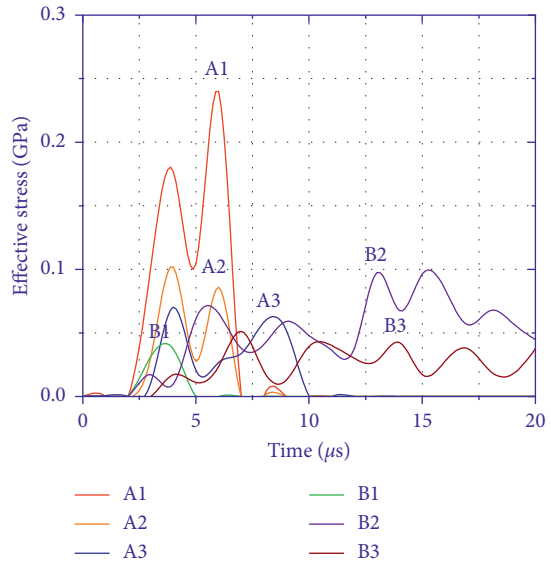

Figure 17: Stress curve of anhydrous bag-charge blasting unit.

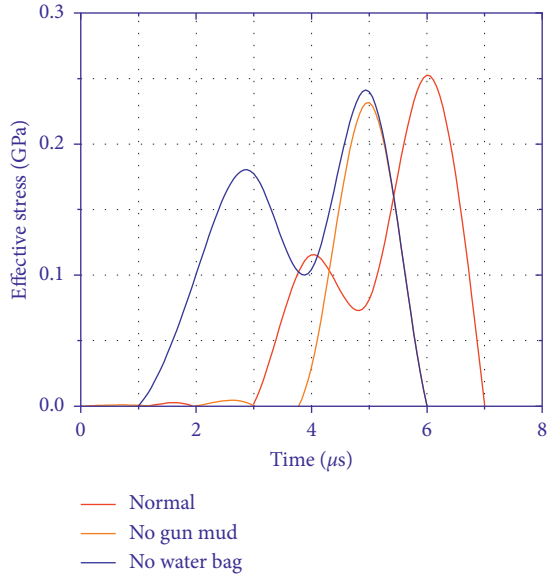

Figure 18: Comparison of maximum stress curves.

blasting mud can prolong blasting stress time and reduce energy waste.

As shown in Figure 19, the maximum value of the shaped charge structure is about $0.21 * 10^{-3}$ cm/μs at the monitoring points in the nongathering direction. The maximum vibration velocity is about $0.25 * 10^{-3}$ cm/μs.

As shown in Figure 20, the maximum vibration velocity was about $0.15 * 10^{-3}$ cm/μs in the nonaccumulating direction. The maximum vibration velocity is about $0.30 * 10^{-3}$ cm/μs. By comparison, the local vibration velocity of nonshot mud-concentrated blasting simulation is large, and the blasting effect is unstable.

As shown in Figure 21, the maximum vibration velocity is about $0.27 * 10^{-3}$ cm/μs. The maximum vibration velocity is about $0.25 * 10^{-3}$ cm/μs in the direction of the nonaccumulator groove. The maximum value of the convergence velocity in the direction of the polyenergy trough is larger than normal. This means that the water bag results in reducing the blast vibration speed.

The above three charge structures show that the nodal ensemble velocity maxima in the aggregation direction is generated at monitoring point A1, and the nonaggregation direction maxima is generated at monitoring point B1. With different charge configurations, the maximum velocity in both directions is generated at the nearest location to the gun hole position. In the same direction, the maximum nodal closing velocity gradually decreases as the distance from the gun hole increases.

As shown in Figure 22, found by comparative analysis, blasting mud-blocking holes can effectively prolong blasting vibration velocity-time, reduce the instantaneous speed, and improve blasting stability. Water bags can store part of the

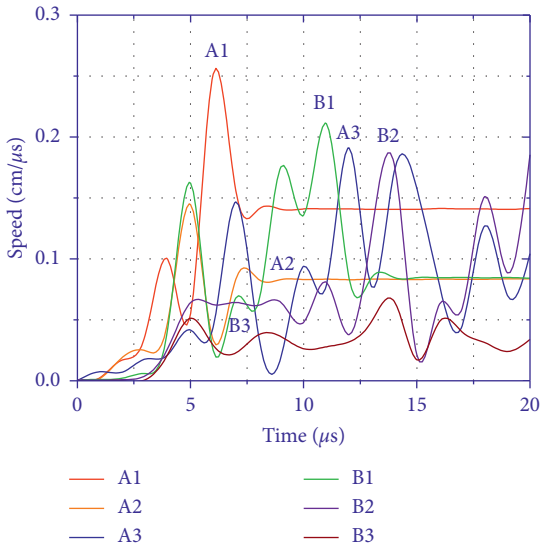

Figure 19: Joint velocity curve of shaped charge hydraulic blasting.

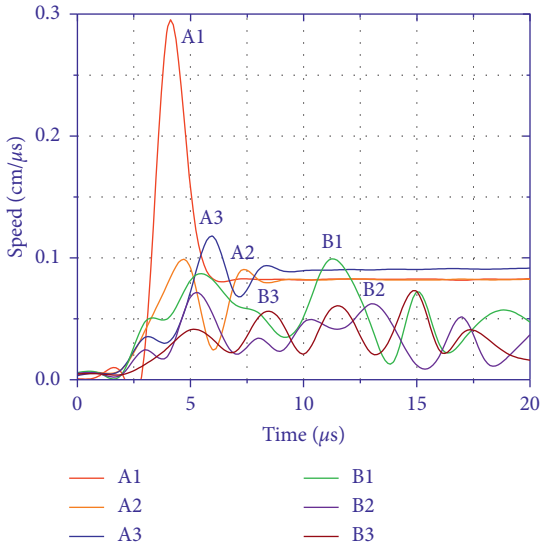

Figure 20: Joint velocity curve of no-shot mud-charge blasting.

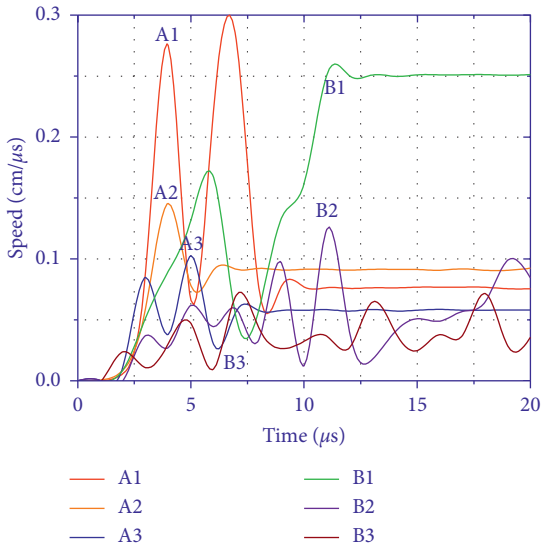

Figure 21: The joint velocity curve of anhydrous bag-charge blasting.

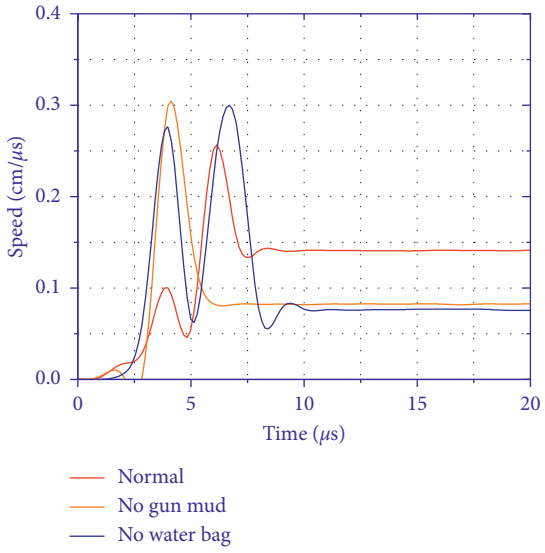

Figure 22: Comparison of maximum velocity curves.

energy to prevent the surrounding rock from being affected by cluttered detonation waves and reduce waste of energy.

As shown in Figure 23, the maximum value of displacement variation in the nonagglomeration direction is about 0.61 cm collected in the nonagglomeration direction by the agglomeration hydrodynamic charge structure. In the direction of aggregation, the maximum displacement variation was collected with a maximum value of about 1.82 cm.

As shown in Figure 24, the maximum value of displacement variation is about 0.25 cm in the nonconcentration direction. In the concentration direction, the maximum value of displacement variation is about 1.79 cm. The final displacement in the agglomerate direction is similar to that in the simulation with gun clay, but the fragmentation of the surrounding rock in the nonagglomerate direction is much less effective, and the blasting effect is not uniform.

As shown in Figure 25, the maximum displacement variation is about 1.69 cm in the aggregation direction. In the nonaggregation direction, the maximum displacement variation is about 1.46 cm. Polyenergy tube polyenergy effect is not obvious, indicating that the water bag in the play of polyenergy tube polyenergy effect has a definite effect.

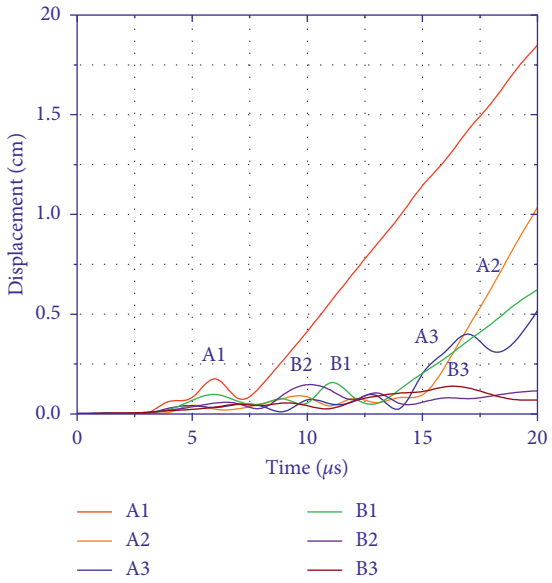

Figure 23: Joint displacement curves of shaped charge hydraulic blasting.

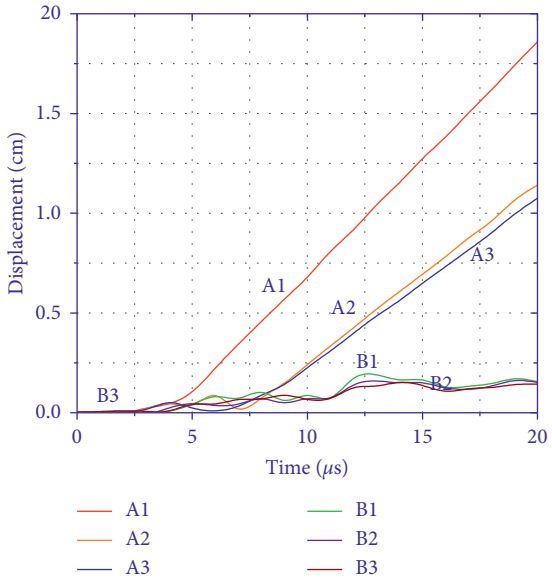

Figure 24: Joint displacement curve of no-slime-charge blasting.

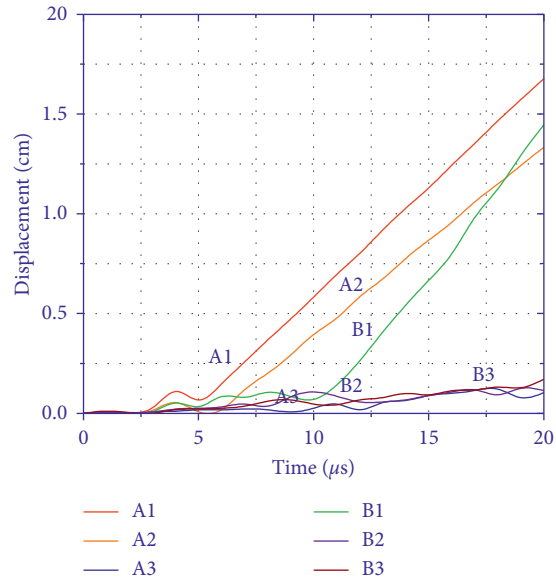

Figure 25: Joint displacement curve of anhydrous bag-charge blasting.

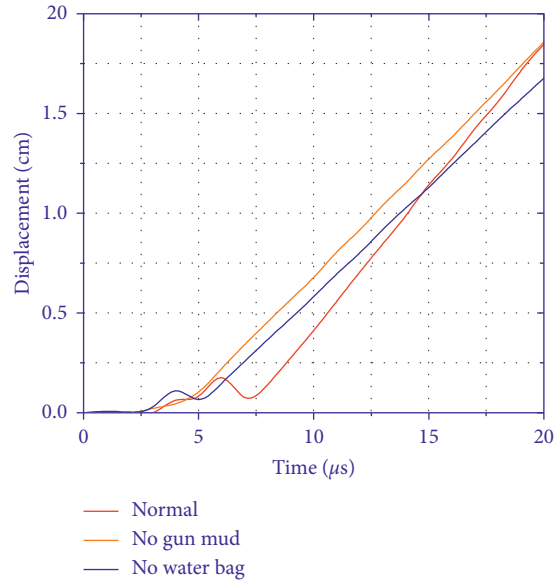

Figure 26: Maximum displacement curve comparison.

The above three charge structures show that the location where the displacement maximum is generated in the concentrated energy direction is monitoring point A1, and the direction where the displacement maximum is generated in the noncollected energy direction is monitoring point B1. It does mean that the maximum displacement in both directions is produced at the position closest to the gun hole. In the same direction, the maximum nodal joint displacement gradually decreases as the distance from the gun hole increases.

As shown in Figure 26, the blasting action time is shorter without gun clay to seal the hole. This indicates that the gun clay can play a role in extending the action time. When blasting without water bags, the maximum displacement of the surrounding rock is relatively small. This indicates that the water pressure can further enhance the blasting effect, and the water bag produces the "water wedge effect."

6. Engineering Applications

Based on the above analysis of the rock-breaking mechanism for the fractured sandstone geological conditions with polyhydrodynamic smooth blasting technology, the corresponding structure of polyhydraulic charge and the hole laying method was designed and applied to Guantian tunnel. The hole layout method is shown in Figure 27, and the hole parameters are given in Table 6.

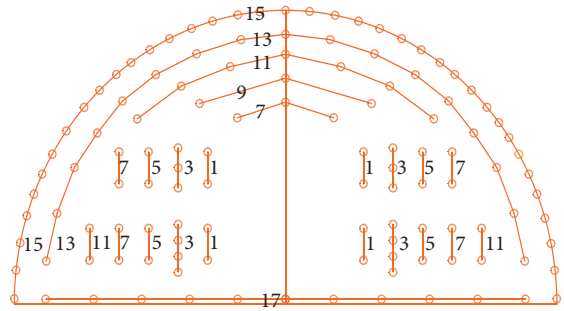

Figure 27: Detonation network diagram of step blasting face.

Table 6: Detailed hole layout parameters.

Gun hole name	Detonator section times	Number of gun holes	Hole deep (m)	Row spacing (cm)	Hole spacing (cm)	Angle (°)	Charging factor	Single hole loading capacity (kg)
Bottom trenching	1	4	1.92	425	80	45	0.56	1.5
	3	8	3.7	585	40	52	0.64	3
	5	4	3.7	745	80	62	0.60	2.4
	7	4	3.7	905	80	78	0.47	1.8
Upper trenching	1	4	1.92	425	80	45	0.56	1.5
	3	6	3.7	585	50	52	0.64	3
	5	4	3.7	745	80	62	0.60	3
	7	4	3.7	905	80	78	0.47	1.8
Auxiliary hole	7	3	3.7	80	100	90	0.57	2.1
	9	3	3.7	60	130	90	0.49	1.8
	11	7	3.7	60	120	90	0.49	1.8
	13	17	3.7	50	90	90	0.41	1.5
Peripheral holes	15	37	3.7	60	70	88	0.84	1.2
Base plate hole	17	11	3.7	85	130	90	0.49	1.8

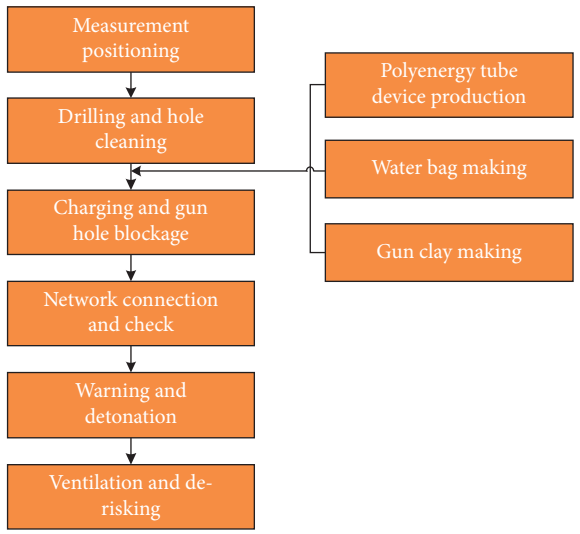

Figure 28: Polyenergy hydrodynamic smooth blasting construction process.

According to the construction design plan, the construction process of polyhydraulic smooth blasting is shown in Figure 28. Based on the above tunnel construction process and gun bore layout parameters, practical engineering applications were carried out in the Guantian tunnel. Good blasting results were obtained in the application. As shown in Figure 29, the arch waist blasting effect and arch top blasting effect are shown respectively.

As shown in Figure 29, the section formed after blasting is flat. The controlled blasting effect of the arch waist and arch top was good. The local maximum overexcavation was 18 cm, and the maximum underexcavation was 10.7 cm, as learned from the analysis of on-site measurement. The retention rate of perimeter hole marks after blasting is above 80%. External blasting vibration velocity has a significant reduction compared with conventional blasting, and the impact of blasting on the surrounding environment is lower.

7. Discussion

In order to avoid the influence of lithology change on the experimental data, two sets of experiments were set on the same horizontal line of the working face to carry out the blasting experiment. This experiment was also based on the geological conditions of the working face. Although a certain safety spacing is set in the layout of different blast holes in separate experimental groups, it cannot fully ensure that the

(a) (b)

Figure 29: Field construction blasting effect. (a) Blasting effect of vault. (b) Blasting effect of arch waist.

blasting effect of blast holes in the blasting process does not affect the blasting effect of adjacent experimental groups. In the process of setting the experimental parameters, the charge used in blasting and the hole spacing of discrete experimental groups have been adjusted accordingly, and the holes in each group are only set up three. There is still a large gap between the charge required to achieve the whole blasting effect of the water pressure smooth blasting on the palm surface. Therefore, in the process of this experiment, the interaction between neighboring groups is ignored, and the rock-breaking mechanism of hydraulic smooth blasting of broken sandstone geological agglomeration under different charge structures is analyzed and studied. The results can fully meet the application requirements and better guide the construction.

The above experiments and simulations show that the mechanism of polyhydraulic blasting in fractured sandstone geological conditions is as follows: In the blasting process of fractured sandstone polyhydraulic smooth blasting, stress waves are first generated by explosive blasting and propagated in the blast holes. With the gradual excitation of the explosive, the pressure inside the hole is increasing part of the pressure propagation to the water body at both ends of the polygon tube, and the energy in the water body begins to increase rapidly. At the same time, the kinetic energy generated by the blast in the direction of the polyglot into potential energy; at this time, the gun clay plays a plugging hole, prolonging the role of explosive gas action time, to promote the full reaction of explosives. After the completion of energy concentration, it starts to generate energy concentration jets along the direction of the energy concentration tank, cutting the rock into seams and fracturing the molecular structure of the rock. At the same time, the water in the cannon hole begins to play the role of "water wedge" along the fusion fracture after the energy storage is completed, so that the fracture can be better extended and extended. Here, this rock-breaking mechanism is explained as the dual rock-breaking mechanism of "concentrated energy jet + water wedge."

8. Conclusions

The following conclusions are obtained through the experimental study on the mechanism of concentrated hydraulic smooth blasting and the finite element numerical analysis:

(1) In the case of joint-hole concentrated blasting, the concentrated jet can easily penetrate the rock to achieve the desired blasting effect. At the same time, less explosive gas will spread along the rock both fractures, and the blasting method can effectively achieve controlled blasting of broken sandstone.

(2) Polyenergy blasting: The use of gun clay to seal the hole can effectively improve the stability of the blasting effect, reduce the waste of explosive gas, and prolong the blasting effect time.

(3) Water bag in the blasting process can enhance the blasting effect through the water wedge effect. At the same time, the water bag has a certain amount of energy storage. In the structure of the charge, the water bag combined with the gun clay can work better.

(4) It is concluded from the research and analysis that the mechanism of rock breaking by polyenergetic water pressure smooth blasting in fractured sandstone geological conditions is the double breaking action of "polyenergetic jet + water wedge action."

(5) In this article, based on the study of blasting mechanism, the deployment method of polyenergy hydropressure smooth blasting is designed, which has been well applied in engineering practice.

Data Availability

The spread sheet data used to support the results of this study will be provided by the author on permission and therefore cannot be provided free of charge. For these data, contact the author: Xu. Zhang.

Conflicts of Interest

The author(s) declare(s) that there are no conflicts of interest regarding the publication of this paper.

Acknowledgments

This study has been partially funded by the National Natural Science Foundation of China (Grant Nos. 520095077 and 51934004), China Scholarship Council (CSC NO. 201608370083), the Natural Science Foundation of Shandong Province (Grant no. ZR2019ZD14), and the "Taishan Scholars Young Expert Program" of Shandong Province China (No. tsqn202103074). These supports are gratefully acknowledged.

References

[1] H. K. Verma, N. K. Samadhiya, M. Singh, R. K. Goel, and P. K. Singh, "Blast induced rock mass damage around tunnels," *Tunnelling and Underground Space Technology*, vol. 71, pp. 149–158, 2018.

[2] E. Hamdi, N. B. Romdhane, and J. M. Le Cléac'h, "A tensile damage model for rocks: application to blast induced damage assessment," *Computers and Geotechnics*, vol. 38, no. 2, pp. 133–141, 2011.

[3] M. Monjezi, M. Ghafurikalajahi, and A. Bahrami, "Prediction of blast-induced ground vibration using artificial neural networks," *Tunnelling and Underground Space Technology*, vol. 26, no. 1, pp. 46–50, 2011.

[4] L. X. Xie, W. B. Lu, Q. B. Zhang, Q. H. Jiang, G. H. Wang, and J. Zhao, "Damage evolution mechanisms of rock in deep tunnels induced by cut blasting," *Tunnelling and Underground Space Technology*, vol. 58, pp. 257–270, 2016.

[5] L. F. Fan, X. W. Yi, and G. W. Ma, "Numerical manifold method (NMM) Simulation of stress wave propagation through fractured rock mass," *International Journal of Applied Mechanics*, vol. 5, no. 2, 2013.

[6] N. Jiang, C. B. Zhou, X. D. Luo, and S. Lu, "Damage characteristics of surrounding rock subjected to VCR mining blasting shock," *Shock and Vibration*, vol. 2015, Article ID 373021, 8 pages, 2015.

[7] F. García Bastante, L. Alejano, and J. González-Cao, "Predicting the extent of blast-induced damage in rock masses," *International Journal of Rock Mechanics and Mining Sciences*, vol. 56, pp. 44–53, 2012.

[8] Y. Hu, W. Lu, M. Chen, P. Yan, and J. Yang, "Comparison of blast-induced damage between presplit and smooth blasting of high rock slope," *Rock Mechanics and Rock Engineering*, vol. 47, no. 4, pp. 1307–1320, 2014.

[9] X. M. Feng, J. Z. Zhuang, J. S. Ju, and X. Jiang, "Smooth blasting hole spacing and smooth surface layer depth optimization," *Advanced Science Letters*, vol. 4, no. 8-10, pp. 2703–2707, 2011.

[10] B. P. Zou, Z. P. Xu, J. X. Wang, Z. Lu, and L. Hu, "Numerical investigation on influential factors for quality of smooth blasting in rock tunnels," *Advances in Civil Engineering*, vol. 2020, Article ID 9854313, 17 pages, 2020.

[11] Z. L. Zhou, R. S. Cheng, X. Cai, J. Jia, and W. Wang, "Comparison of presplit and smooth blasting methods for excavation of rock wells," *Shock and Vibration*, vol. 2019, Article ID 3743028, 12 pages, 2019.

[12] X. P. Li, J. L. Lv, J. H. Huang, Y. Lu, and T. T. Lu, "Numerical simulation research of smooth wall blasting using the timing sequence control method under different primary blast hole shapes," *Shock and Vibration*, vol. 2019, Article ID 2425904, 16 pages, 2019.

[13] K. Liu and B. Liu, "Optimization of smooth blasting parameters for mountain tunnel construction with specified control indices based on a GA and ISVR coupling algorithm," *Tunnelling and Underground Space Technology*, vol. 70, pp. 363–374, 2017.

[14] X. P. Li, J. H. Huang, Y. Luo, and P. P. Chen, "A study of smooth wall blasting fracture mechanisms using the Timing Sequence Control Method," *International Journal of Rock Mechanics and Mining Sciences*, vol. 92, pp. 1–8, 2017.

[15] Z. Zhou, X. Cai, D. Ma et al., "Water saturation effects on dynamic fracture behavior of sandstone," *International Journal of Rock Mechanics and Mining Sciences*, vol. 114, pp. 46–61, 2019.

[16] H. Jiang, Z. Liu, and K. Gao, "Numerical simulation on rock fragmentation by discontinuous water-jet using coupled SPH/FEA method," *Powder Technology*, vol. 312, pp. 248–259, 2017.

[17] A. W. Momber, "The response of geo-materials to high-speed liquid drop impact," *International Journal of Impact Engineering*, vol. 89, pp. 83–101, 2016.

[18] Y. Liu, J. Wei, and T. Ren, "Analysis of the stress wave effect during rock breakage by pulsating jets," *Rock Mechanics and Rock Engineering*, vol. 49, no. 2, pp. 503–514, 2016.

[19] B. Huang, C. Liu, J. Fu, and H. Guan, "Hydraulic fracturing after water pressure control blasting for increased fracturing," *International Journal of Rock Mechanics and Mining Sciences*, vol. 48, no. 6, pp. 976–983, 2011.

[20] Q. Ye, Z. Jia, and C. Zheng, "Study on hydraulic-controlled blasting technology for pressure relief and permeability improvement in a deep hole," *Journal of Petroleum Science and Engineering*, vol. 159, pp. 433–442, 2017.

[21] S. Y. Liu, Y. M. Cui, S. Cui, Z. Li, F. Zhou, and H. Wang, "Experimental investigation on rock fracturing performance under high-pressure foam impact," *Engineering Fracture Mechanics*, vol. 252, Article ID 107838, 2021.

[22] Y. Wang, "Analysis of dynamic characteristics of through-wall cracks between 2 boreholes in the directed fracture controlled blasting," *Fatigue and Fracture of Engineering Materials and Structures*, vol. 41, no. 2, pp. 273–286, 2018.

[23] R. Yang, Y. Wang, and C. Ding, "Laboratory study of wave propagation due to explosion in a jointed medium," *International Journal of Rock Mechanics and Mining Sciences*, vol. 81, pp. 70–78, 2016.

[24] B. Wang, H. B. Li, Z. S. Shao, S. Chen, and X. Lu, "Investigating the mechanism of rock fracturing induced by high-pressure gas blasting with a hybrid continuum-discontinuum method," *Computers and Geotechnics*, vol. 140, Article ID 104445, 2021.

[25] C. X. Ding, R. S. Yang, Z. Lei, and M. Wang, "Fractal damage and crack propagation in decoupled charge blasting," *Soil Dynamics and Earthquake Engineering*, vol. 141, no. 4, Article ID 106503, 2020.

[26] X. M. Lou, Z. C. Wang, B. G. Chen, and J. Yu, "Theoretical calculation and experimental analysis on initial shock pressure of borehole wall under axial decoupled charge," *Shock and Vibration*, vol. 2018, Article ID 7036726, 14 pages, 2018.

[27] Y. Luo and Z. W. Shen, "Application study on directional fracture controlled blasting with shaped charge in rock," *Explosion and Shock Waves*, vol. 13, no. 3, pp. 193–198, 2006.

[28] Y. Yin, Q. Sun, B. Zou, and Q. Mu, "Numerical study on an innovative shaped charge approach of rock blasting and the timing sequence effect in microsecond magnitude," *Rock Mechanics and Rock Engineering*, vol. 54, no. 9, pp. 4523–4542, 2021.

[29] H. L. Yan, "Research and application of concentrated water pressure smooth blasting in long mountain tunnel," *Shandong University of Science and Technology*, vol. 136, Article ID 04038, 2020.

[30] H. D. Liang, P. F. Guo, and D. J. Sun, "Study on stress wave propagation and crack expansion law of different polyenergy blasting modes," *Vibration and Shock*, vol. 39, no. 4, pp. 157–164+184, 2020.

[31] J. G. Li and K. Yang, "Application of the second-generation polyenergy tube hydrodynamic smooth blasting technology in the Lower Guili Tunnel," *Modern Tunnel Technology*, vol. 57, no. S1, pp. 1035–1041, 2020.

[32] Y. Q. Song, S. Li, and D. Y. Guo, "Numerical simulation and application of multi-hole homogeneous polyenergy blasting coal seam penetration enhancement," *Journal of Coal*, vol. 43, no. S2, pp. 469–474, 2018.

[33] S. C. Duane, B. Khahn, and K. Christian, "Implementation and validation of the johnson-holmquist ceramic material model in LS dyna," in *Proceedings of the 4th European LS-Dyna Users Conference*, Ulm, Germany, May 22-23, 2003.

[34] K. Liu, C. Q. Wu, X. B. Li, Q. Li, J. Fang, and J. Lin, "A modified HJC model for improved dynamic response of brittle materials under blasting loads," *Computers and Geotechnics*, vol. 123, Article ID 103584, 2020.